Revista Brasileira de Geofísica
RBGf
Brazilian Journal of Geophysics

Revista Brasileira de Geofísica (2017) 35(3): 163-171

ISSN 0102-261X
www.scielo.br/rbg

APPLICATION OF ISO-FREQUENCY MAPS TO TIME-LAPSE DATA

Wagner Moreira Lupinacci[1], Anderson Peixoto de Franco[2],
Fernando Vizeu Santos[1] and Marco Antonio Cetale Santos[1]

ABSTRACT. Time-frequency transforms are widely used in seismic exploration. These transforms enable analysis of the energy density of a non-stationary signal as functions of amplitude, time and frequency. The representation of energy density is not unique, and each transform has its advantages and disadvantages. The choice of which transform should be used depends on the application. In this paper, we propose a new way to analyze time-lapse anomalies using iso-frequency panels obtained by time-frequency transforms. We compared the iso-frequency panels of the Morlet Wavelet Transform and Choi-Williams Distribution. These panels revealed different characteristics and can provide additional information for the interpretation of time-lapse anomalies. We used seismic data from the Marimbá field of the Campos Basin, Brazil, for which base and monitor acquisitions were held in 1984 and 1999, respectively. We also used a special filtering approach to enhance seismic resolution and remove noise, whereby we applied the curvelet transform to remove noise, and employed a tool to correct the residual moveout and inverse Q filtering for attenuation correction. Then we analysed the time-lapse anomalies using iso-frequency panels. The main time-lapse anomalies appeared in the form of clouds in the iso-frequency panels obtained by the Morlet Wavelet Transform approach. Iso-frequency panels obtained by Choi-Williams Distribution showed a higher sensitivity and resolution for analyzing the anomalies. Our results show the great potential of these transforms for visualization of time-lapse anomalies.

Keywords: time-lapse anomalies, spectrogram, Morlet Wavelet Transform, Choi-Williams Distribution.

RESUMO. Transformadas tempo-frequência são amplamente utilizadas na exploração sísmica. Estas transformadas permitem a análise da densidade de energia de um sinal não-estacionário como funções de amplitude, tempo e frequência. A representação da densidade de energia de um sinal não é única, e cada transformada tem suas vantagens e desvantagens. A escolha da transformada que deve ser usada depende da aplicação. Neste artigo, propomos uma nova abordagem para analisar anomalias de dados *time-lapse* usando painéis iso-frequência obtidos através de transformadas tempo-frequência. Comparamos os painéis iso-frequência obtidos com a Transformada Wavelet de Morlet e a Distribuição de Choi-Williams. Estes painéis revelaram diferentes características que podem fornecer informações adicionais para a interpretação de anomalias *time-lapse*. Os dados sísmicos utilizados foram do Campo de Marimbá da Bacia de Campos, Brasil, os quais as aquisições base e monitor foram realizadas em 1984 e 1999, respectivamente. Antes da análise dos painéis iso-frequência, usamos um *workflow* para melhorar a resolução sísmica e a razão sinal-ruído. Neste *workflow*, aplicamos a Transformada Curvelet para remover ruídos aleatórios e coerentes, uma ferramenta para corrigir o *moveout* residual e um Q*-filter* para correção dos efeitos da atenuação. Após este *workflow*, as principais anomalias *time-lapse* apareceram na forma de nuvens nos painéis iso-frequência da Transformada Wavelet de Morlet. Já os painéis iso-frequência da Distribuição de Choi-Williams apresentaram uma maior sensibilidade e resolução para análise dessas anomalias. Os resultados mostraram o grande potencial dessas transformadas para a visualização e interpretação de anomalias *time-lapse*.

Palavras-chave: anomalias *time-lapse*, espectrograma, Transformada Wavelet de Morlet, Distribuição de Choi-Williams.

[1]Universidade Federal Fluminense, (UFF/LAGEMAR), Av. Gen. Milton Tavares de Souza, s/n, Boa Viagem, 24210-346 Niterói, RJ, Brazil. Phone: +55(21) 2629-5918; +55(21) 99848-2700 – E-mails: wagnerlupinacci@id.uff.br; fvizeus@gmail.com; marcocetale@id.uff.br

[2]Invison Geophysics, Rua Barra do Piraí, 387, Casa 01, Jardim Mariléa, 28895-895 Rio das Ostras, RJ, Brazil. Phone: +55(21) 2760-6902 – E-mail: awpfranco@gmail.com

INTRODUCTION

Time-frequency transforms decompose temporal signals into energy density maps. These maps highlight features that are difficult to see in the time domain. There are many decomposition procedures and, consequently, a temporal signal can undergo different time-frequency analyses. There is more than one method available to express the energy of the signal as a function of time and frequency. Each method has its advantages and disadvantages, and different applications require different transforms (Castagna & Sun, 2006). In seismic exploration, these decompositions have been used for stratigraphic mapping (Partyka et al., 1999), gas reservoir detection (Castagna et al., 2003), carbonate reservoir characterization (Li et al., 2011), ground roll attenuation (Liu & Fomel, 2013), and attenuation estimation and correction (Lupinacci & Oliveira, 2015).

Linear transforms decompose the signal into orthogonal basis functions. These transforms obey the Heisenberg uncertainty principle, which says that a higher frequency resolution causes a smaller temporal resolution, and vice-versa (Addison, 2002). The Continuous Wavelet Transform (CWT) belongs to this class. Sinha et al. (2005) developed a methodology for computing a time-frequency map for nonstationary signals using the CWT and applied it to hydrocarbon zone detection and channel identification.

Decompositions based on linear transformations often fail to obtain simultaneously good temporal and frequency resolutions due to the limitations imposed by the Heisenberg uncertainty principle. In bilinear transforms, the base functions of the spectral decomposition are not necessarily orthogonal. These transforms decompose the signal into biorthogonal basis functions. This can result in better temporal and frequency resolutions. The Wigner-Ville Distribution (WVD) is a prime example of this type of transform. However, the cross-term interference produced by this transform make it difficult to analyze the signal in the time-frequency domain. Choi & Williams (1989) tackled this problem by using an exponential kernel function to reduce the cross-term interference; this transform is known as the Choi-Williams Distribution (CWD). Wu & Liu (2009) used the WVD with a Gauss kernel function (smoothed pseudo Wigner-Ville Distribution) to detect low-frequency shadows caused by hydrocarbons and to delineate the space distribution of anomalous geological bodies more precisely.

Matching Pursuit Decomposition (MPD), introduced by Mallat & Zhang (1993), decomposes signal into a linear expansion of waveforms belonging to functions dictionary. These waveforms, which are generally not orthogonal functions, are frequently chosen in order to best match the signal structures, thereby achieving a better representation of the signal. Rojas (2008) analyzed MPD attributes on time-lapse multicomponent seismic data and he was able to identify the faults and fractures through which gas was migrating to upper reservoirs. The main disadvantage of the MPD approach is the high computational cost to decompose the signal.

In this article, we propose a new alternative to analyze time-lapse seismic anomalies. For this, we use the iso-frequency amplitudes obtained by the Morlet Wavelet Transform (MWT) and Choi-Williams Distribution (CWD). We applied this methodology to data from the Marimbá field and revealed different characteristics that provide additional information for the interpretation of time-lapse anomalies.

METHODOLOGY

A continuous wavelet transform decomposes a signal into family functions (wavelets), which are obtained from an elementary function (mother wavelet) via dilation and translation. The representation of wavelets derived from a mother wavelet is given as (Addison, 2002):

$$\psi_{a,b}(t) = \frac{1}{\sqrt{a}}\psi\left(\frac{t-b}{a}\right), \qquad (1)$$

where a and b are the dilation and translation parameters, respectively, and the mother wavelet $\psi(t)$ has $a = 1$ and $b = 0$. The wavelet transform is defined as the inner product of a signal, $x(t)$, with the wavelet function:

$$T(a,b) = \int_{-\infty}^{\infty} x(t)\psi^*_{a,b}dt\,. \qquad (2)$$

The asterisk indicates that the complex conjugate of the wavelet transform is used in the transform. There are several wavelets that can be used as a mother wavelet, one of which is the complex Morlet Wavelet, defined as:

$$\psi\left(\frac{t-b}{a}\right) = \pi^{-1/4}e^{i2\pi f_0(t-b)/a}e^{-[(t-b)/a]^2/2}, \qquad (3)$$

where $\pi^{-1/4}$, f_0, $e^{i2\pi f_0(t-b)/a}$ and $e^{-[(t-b)/a]^2/2}$ are the normalization factor, center frequency, complex harmonic and a Gaussian envelope, respectively. The center frequency of the mother wavelet, f_0, can be used as reference ($a = 1$) to convert the scale parameter to a characteristic frequency, f. The center frequency is given when the wavelet spectral amplitude is maximal. Since the spectral components are inversely proportional to the dilation, the characteristic frequency of an arbitrary wavelet is inversely proportional to the scale parameter, i.e. $f = f_0/a$.

The time-frequency distribution (map) of a signal's energy density is also called a spectrogram. Representation of the

spectrogram using the CWT can be given as:

$$\mathbf{A}_{wc}(\mathbf{t},\mathbf{f}) = \iint |T(t,f;\psi)|^2 dtdf\,. \quad (4)$$

where $T(t,f;\psi)$ is Eq. 2 with the scale parameter replaced by the characteristic frequency and, in our application, ψ is the complex Morlet Wavelet (Eq. 3).

The Wigner-Ville Distribution (WVD) is obtained by a Fourier transformation of the product between the analytical signal and its conjugate value. This distribution can obtain good resolution for both the frequency and time domains simultaneously. However, applications using WVD are hampered by cross-terms interference, which can be suppressed using an appropriate kernel function. The Choi-Williams Distribution uses an exponential kernel function to ameliorate the occurrence of cross-terms, and is defined as:

$$\mathbf{A}_{cw}(\mathbf{t},\mathbf{f}) = \iint B(\eta,\tau)\phi(\eta,\tau)e^{i2\pi(\eta t-\tau f)}d\eta d\tau\,, \quad (5)$$

with:

$$B(\eta,\tau) = \int x\left(t+\frac{\tau}{2}\right)\bar{x}\left(t-\frac{\tau}{2}\right)e^{i2\pi\eta t}dt\,, \quad (6)$$

and the kernel function:

$$\phi(\eta,\tau) = e^{-\alpha(\eta\tau)^2}\,, \quad (7)$$

where α is an adjust parameter. This kernel function filters the cross-terms that differ in both the time and frequency centers, but cannot do anything regarding cross-terms along the η and τ axes in the ambiguity domain (Cohen, 1989).

From the time-frequency distribution, we obtain the iso-frequency amplitudes:

$$\mathbf{A}_{\mathrm{iso}} = \mathbf{A}(\boldsymbol{\tau}, f_c)\,, \quad (8)$$

where $\mathbf{A}(\boldsymbol{\tau}, f_c)$ are spectrogram amplitudes along time $\boldsymbol{\tau}$ for a constant frequency value, f_c. In our application, we used the MWT, $\mathbf{A}_{WC}$, and CWD, $\mathbf{A}_{CW}$, to obtain the iso-frequency amplitudes, $\mathbf{A}_{\mathrm{iso}}$.

SYNTHETIC DATA RESULTS

The synthetic seismic traces were modeled using the convolution model of a random reflectivity function with a Ricker wavelet. Attenuation effects were added using the constant Q model (Kjartansson, 1979). We simulated a substitution fluid, varying the reflection coefficients by 10% and using a Q factor of 80 to 100 in a small area of the base seismic trace to model the monitor seismic trace. These seismic traces are shown in Figure 1, with the region between the green bars defining where simulation of fluid substitution occurred. The differences between the base and monitor seismic traces are due to the changes in the reflection coefficients and in the Q factor, as shown in Figures 1c and 1d, respectively. The time-lapse seismic trace resulting from summation of these two effects is displayed in Figure 1e. In this example, it is apparent that anomalies caused by changes in the Q factor tend to be small, making it difficult to analyze variation in this attribute for time-lapse seismic data.

MWT spectrograms of the base and time-lapse seismic traces are shown in Figure 2. Using MWT, the energy density decay, caused by attenuation, is smooth and uniform (Fig. 2b). In the time-lapse seismic trace spectrogram (Fig. 2d), we noticed that the anomaly began before and ended after the region where simulation of the fluid substitution occurred.

In Figure 3, we visualize the CWD spectrograms of the base and time-lapse seismic traces. These spectrograms show a strong ability to focus on the moments when events actually happened. However, the energy density decay is neither smooth nor uniform (Fig. 3b). Anomalies in the time-lapse seismic trace spectrogram are concentrated in the area where are the greatest contrasts in seismic amplitudes, demonstrating the high temporal and frequency resolutions of this transform (Fig. 3d).

In the MWT, the parameter that controls the frequency and temporal resolutions is the product of the temporal window length and the frequency band length. In the CWD, the energy density is controlled by the kernel function length and the time and frequency smoothing windows. These windows help reduce the influence of cross-terms. In our application, we used time and frequency Gaussian windows. In the synthetic data, the parameters of the transforms were adjusted to produce only variations in the iso-frequency amplitudes in the fluid substitution region.

Figure 4 shows the time-lapse seismic trace and iso-frequency amplitudes with $f_c = 10$Hz and $f_c = 30$Hz obtained by the MWT and CWD spectrograms. The iso-frequency amplitudes are always positive when the MWT is used. These amplitudes had a form similar to that of a Gaussian with $f_c = 10$Hz (Fig. 4b) and also had lower amplitudes than the iso-frequency amplitudes with $f_c = 30$Hz (Fig. 4c). When we use CWD, the iso-frequency amplitudes can have both positive and negative values. Amplitudes at a lower frequency (Fig. 4d) had variations and absolute values higher than those at a higher frequency $f_c = 15$Hz (Fig. 4e). We noticed good similarity between the time-lapse seismic trace and the iso-frequency amplitudes obtained by CWD.

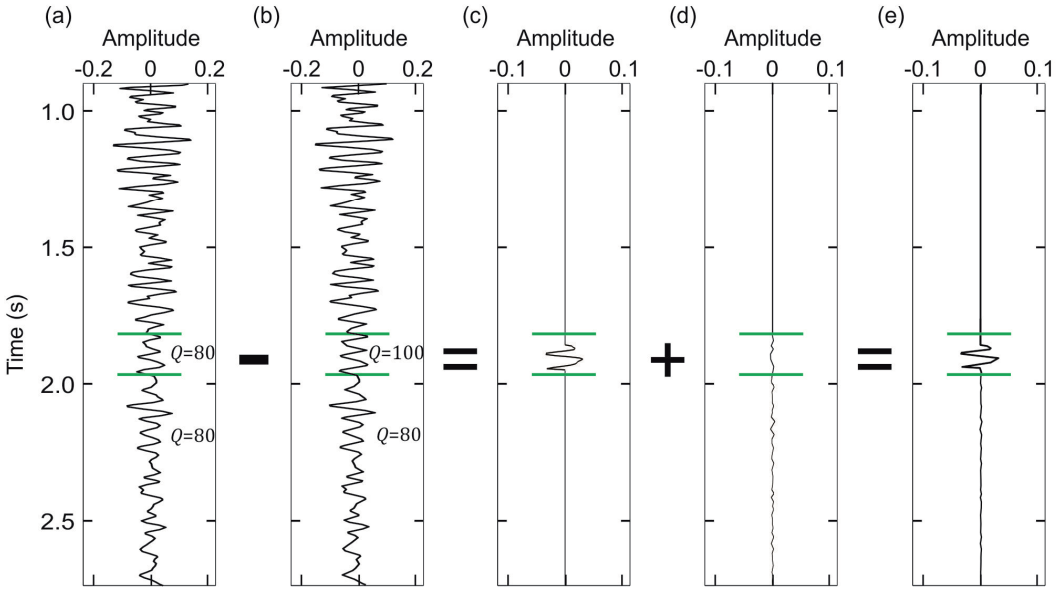

Figure 1 – The two green bars delimit the region where simulation of fluid substitution occurred. (a) The base seismic trace; (b) the monitor seismic trace; (c) and (d) are the result of differences between the base and monitor seismic traces due to changes in the reflection coefficients and in the Q factor, respectively; (e) the time-lapse seismic trace.

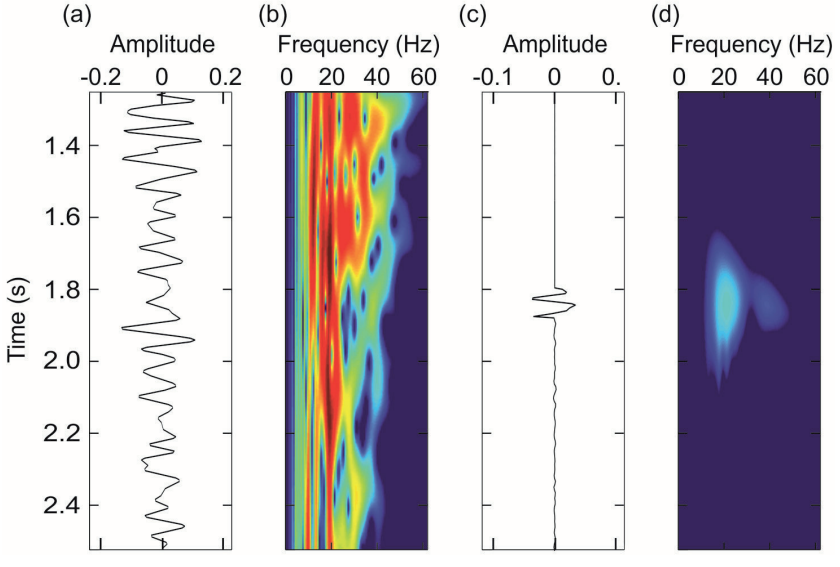

Figure 2 – (a) The base seismic trace; (b) the MWT spectrogram of the base seismic trace; (c) the time-lapse seismic trace; (d) the MWT spectrogram of the time-lapse seismic trace.

REAL DATA RESULTS

The time-lapse seismic data used in this study are from the Marimbá field, which is located in the Campos Basin, about 90 km southeast of São Tomé, off the coast of Rio de Janeiro state (Brazil), in water depths between 320 and 780 m. The Marimbá field reservoirs are turbiditic sandstones of the Carapebus Formation (Bizzi et al., 2003). The base and monitor acquisitions with streamers were acquired in 1984 and 1999, respectively. The data and monitor seismic sections were obtained through a processing flow consisting of geometrical spread correction, deconvolution, velocity analysis, parabolic Radon demultiple, dip-moveout correction, common offset prestack migration (Stolt), bandpass filtering and cross-equalized amplitude spectrum. After process-

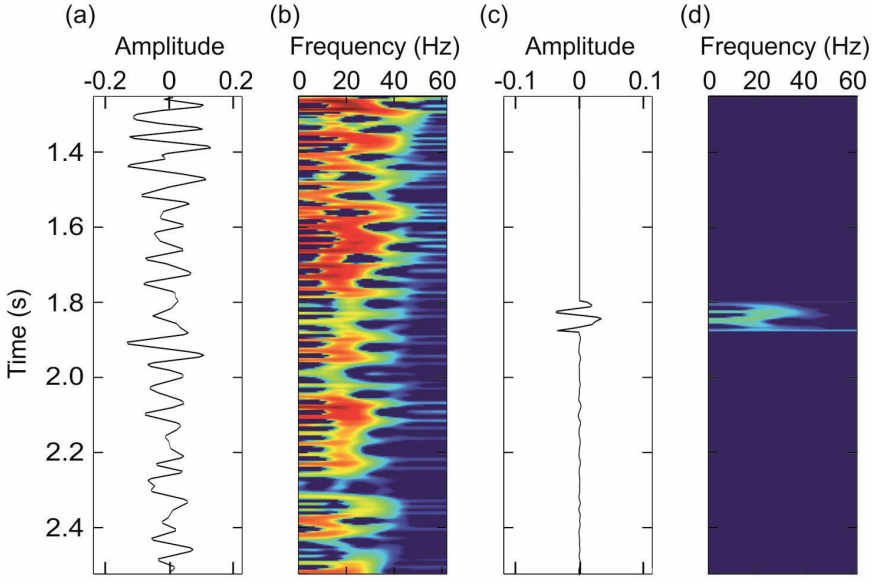

Figure 3 – (a) The base seismic trace; (b) the CWD spectrogram of the base seismic trace; (c) the time-lapse seismic trace; (d) the CWD spectrogram of the time-lapse seismic trace.

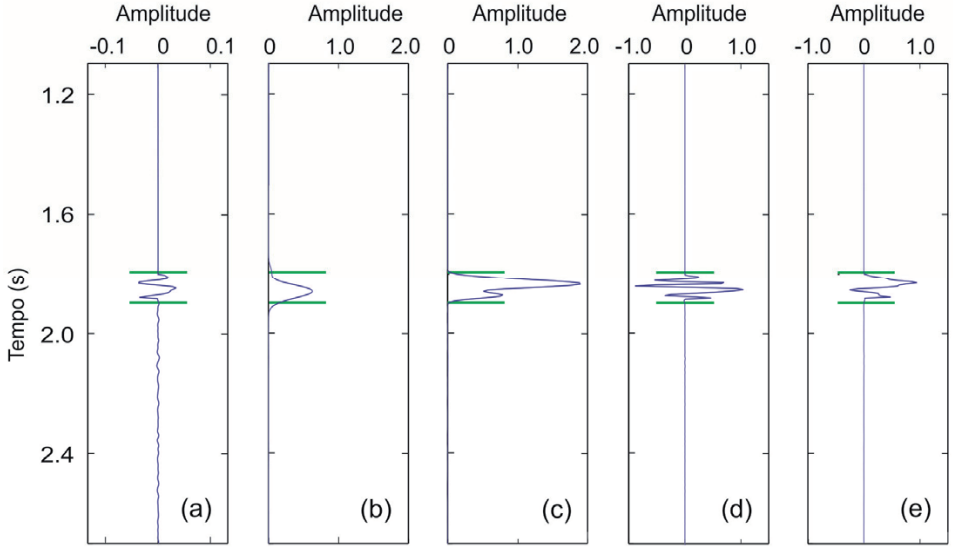

Figure 4 – (a) The time-lapse seismic trace; (b) and (c) are, respectively, the iso-frequency amplitudes with $f_c = 10$Hz and $f_c = 30$Hz obtained by MWT of the time-lapse seismic trace; (d) and (e) are, respectively, the iso-frequency amplitudes with $f_c = 10$Hz and $f_c = 30$Hz obtained by CWD of the time-lapse seismic trace.

ing, we used special filtering tools to enhance seismic resolution and to remove noise with the aim of improving interpretation of the time-lapse anomalies. The special filtering involved the application of three tools. In the first stage, filtering based on a curvelet transform was applied to remove noise (Candès et al., 2006). Then, we used a wavelet-based residual moveout tool (WRMO). In the last stage, we applied a stable inverse Q filtering for attenuation correction. For more details about these tools, see Braga & Moraes (2013), Franco et al. (2015) and Lupinacci & Oliveira (2015). While all these treatments are carried out to improve the signal-to-noise ratio, it is important to preserve the amplitudes so as not to overtly bias results. Thus, we performed

a quality control at each stage for the preservation of signal. The base and monitor seismic sections after application of the filtering tools are shown in Figure 5.

The time-lapse seismic section used to analyze the iso-frequency panels is presented in Figure 6. In this section, a well is located in seismic trace 500. The tops of the two reservoirs present in this well are at depths corresponding to times of 2.60s and 2.70s. We noticed that most of the time-lapse anomalies in Figure 6 are concentrated in the regions of the reservoirs.

Iso-frequency panels of the time-lapse seismic section obtained from the MWT are displayed in Figure 7. We selected a low-frequency panel ($f_c = 10$Hz, Fig. 7a) and a high-frequency panel ($f_c = 30$Hz, Fig. 7b) to analyze the time-lapse anomalies in the MWT iso-frequency panels. The iso-frequency panels obtained from the CWD are shown in Figure 8. The panel with the lowest frequency ($f_c = 5$Hz, Fig. 8a) was chosen in order to produce a panel with characteristics similar to the time-lapse seismic section. The panel with a higher frequency was selected so as to have only positive anomalies ($f_c = 15$Hz, Fig. 8b).

DISCUSSION

In the time-lapse seismic section (Fig. 6), the upper reservoir has higher anomalies than in the lower reservoir. More significant changes in pressure and saturation and a release of more soluble gas during production in the upper reservoir may explain this finding. Anomalies are also apparent near the areas with geological faults. Faults make seismic processing more difficult

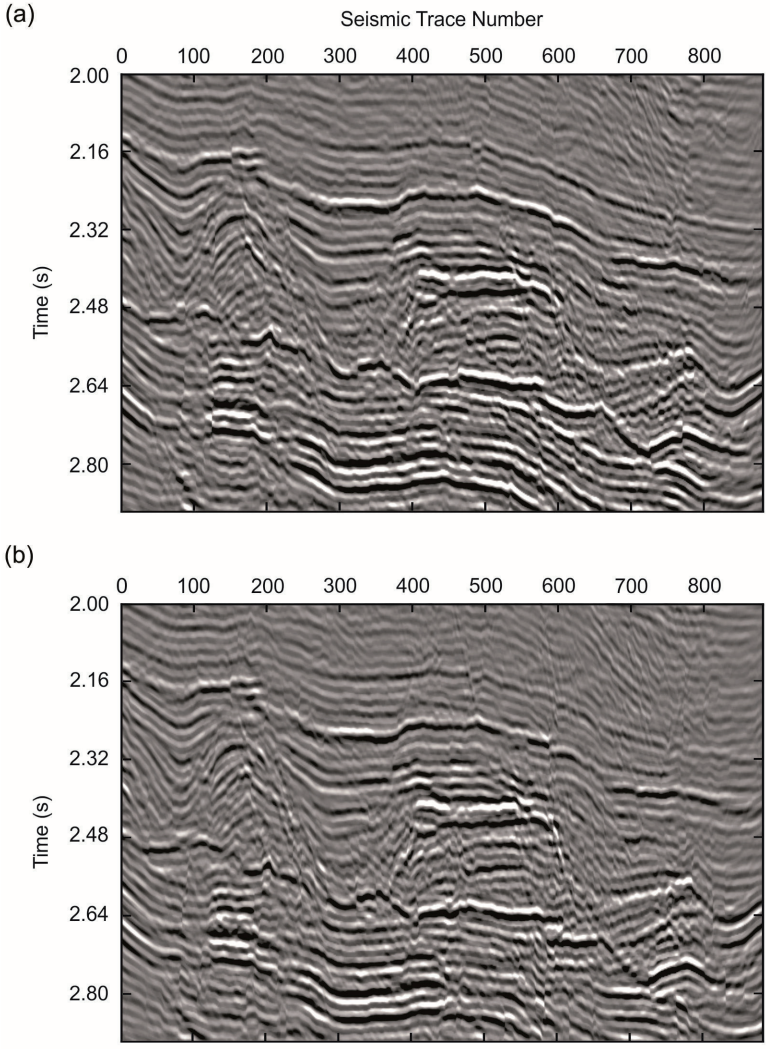

Figure 5 – (a) and (b) are, respectively, the base and monitor seismic data of the Marimbá field after processing and special filtering.

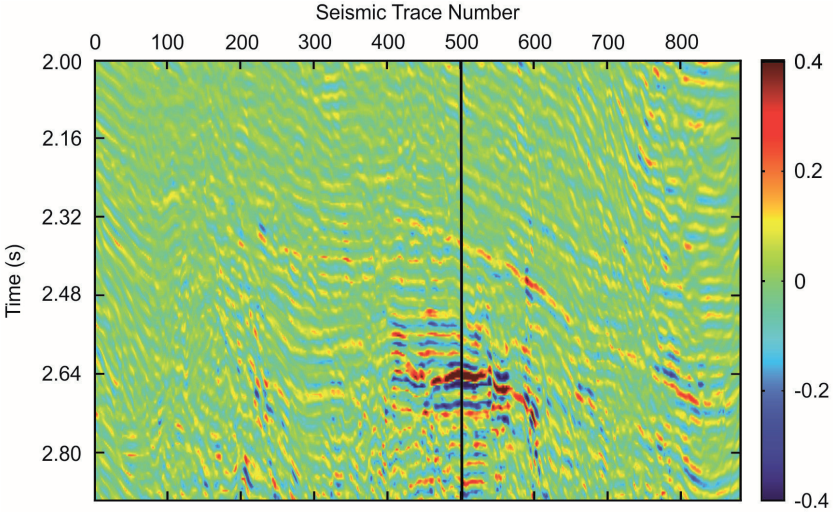

Figure 6 – Time-lapse seismic section of the Marimbá field.

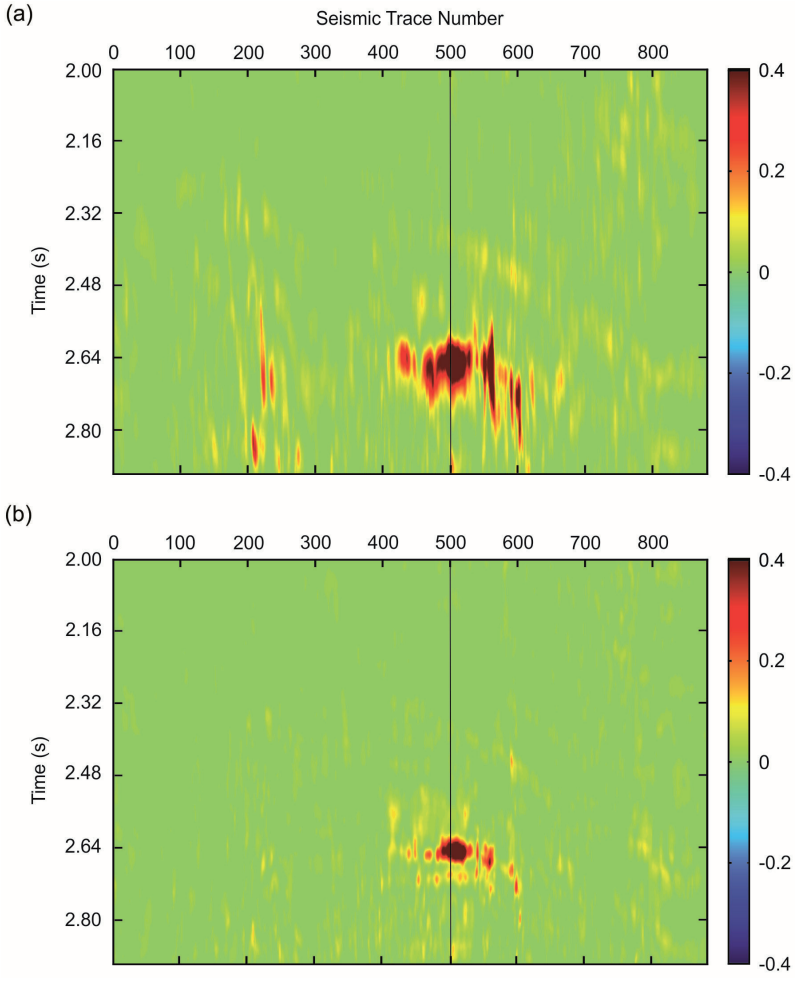

Figure 7 – (a) and (b) are, respectively, the MWT iso-frequency amplitudes of the time-lapse seismic data, with $f_c = 10$Hz and $f_c = 30$Hz.

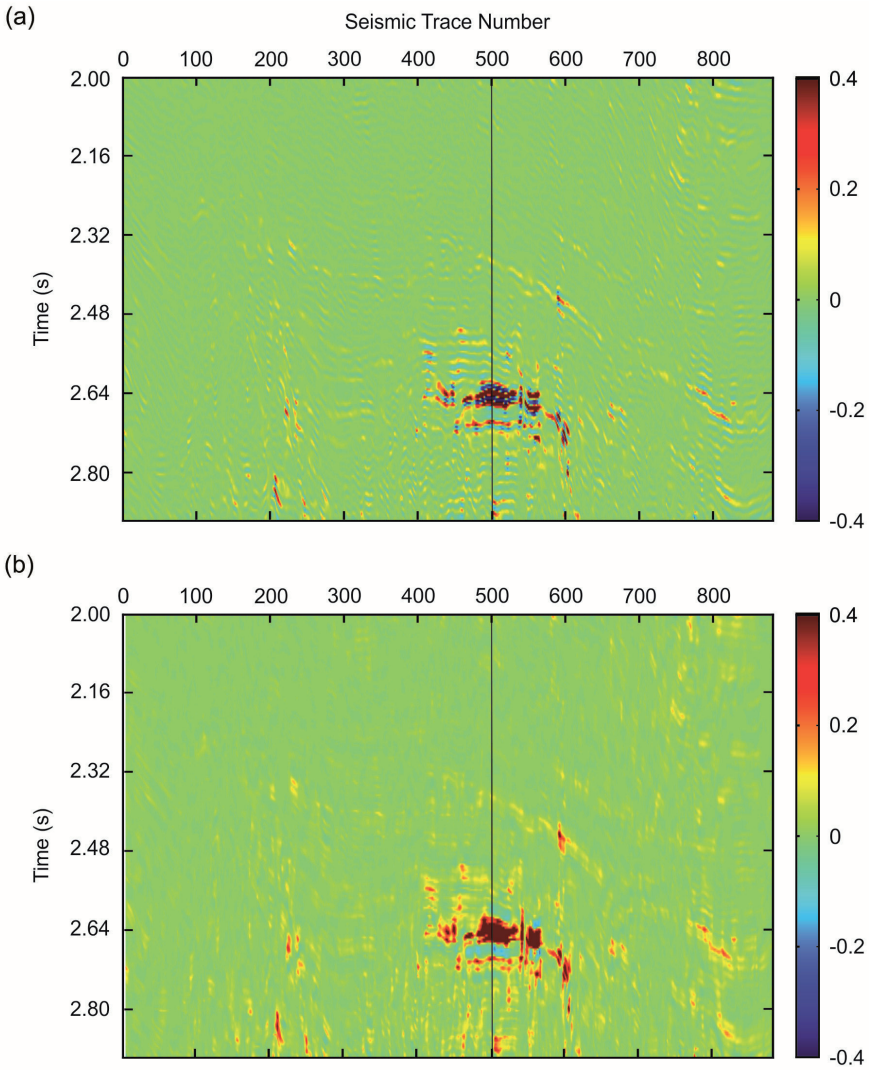

Figure 8 – (a) and (b) are, respectively, the CWD iso-frequency amplitudes of the time-lapse seismic data, with $f_c = 5$Hz and $f_c = 15$Hz.

and can impact the repeatability of time-lapse data, which can cause anomalies that are not associated with fluid substitution.

The iso-frequency panels proved to be less noisy than the time-lapse seismic section, which contributed to better identification of the main anomalies. In all the iso-frequency panels, the anomalies in the reservoir areas were preserved and only in the first MWT panel (Fig. 7a) was it not possible to separate the anomalies detected in the two reservoirs.

In Figure 7b, small circular anomalies can be seen under the main anomalies. In this same region in Figures 8a and 8b, these anomalies appear to have greater lateral continuity due to the higher temporal and frequency resolution of the CWD. These weaker anomalies are in the lower reservoir region and are probably related to small variations in pressure and saturation caused by lower production compared to the upper reservoir.

Anomalies are more distinct in the high-frequency MWT iso-frequency panels than for those of lower frequencies. The real part of MWT transform provides only positive values of spectrogram amplitudes, so we could not determine if the seismic anomalies were caused by positive or negative contrast of the seismic amplitudes. As a consequence, the anomalies often appeared in the form of clouds.

In the CWD iso-frequency panel with $f_c = 5$Hz (Fig. 8a), it is possible to distinguish some anomalies with positive and negative amplitudes. Some anomalies were most clearly defined in the reservoir regions, which contributed to better data interpretation.

The MWT iso-frequency panel with the highest frequency (Fig. 8b) only had positive amplitudes. Thus, by increasing the frequency, the amplitudes of these panels can become solely positive, with good definition of the main anomalies.

CONCLUSION

Our MWT and CWD iso-frequency panels produced an image that was less noisy than the seismic time-lapse section. The weak anomalies and noise were attenuated, and this contributed to better interpretation of the anomalies actually associated with the fluid substitution. In the MWT iso-frequency panels, the anomalies appeared in cloud form and, at higher frequencies, these anomalies were more defined but still had a low resolution. The CWD iso-frequency panels presented anomalies with high resolution, especially using a lower frequency. Our results show the great potential of using time-frequency transforms to analyze time-lapse data.

ACKNOWLEDGEMENTS

The authors thank the Agência Nacional do Petróleo, Gás Natural e Biocombustíveis (ANP – Brazilian Petroleum Agency) for providing the seismic data used in this research.

REFERENCES

ADDISON PS. 2002. The Illustrated Wavelet Transform Handbook. Introductory Theory and Application in Science, Engineering, Medicine and Finance. Napier University, Edinburgh, UK. doi: 10.1088/0305-4470/37/5/B01.

BIZZI LA, SCHOBBENHAUS C, VIDOTTI RM & GONÇALVES JH. 2003. Geologia, Tectônica e Recursos Minerais do Brasil: texto, mapas & SIG. Brasília, Brazil. Serviço Geológico do Brasil-CPRM.

BRAGA ILS & MORAES FS. 2013. High-resolution gathers by inverse Q filtering in the wavelet domain. Geophysics, 78: V53–V61. doi: 10.1190/GEO2011-0508.1.

CANDÈS E, DEMANET L, DONOHO D & YING L. 2006. Fast discrete curvelet transforms. Society for Industrial and Applied Mathematics, Multiscale Model. Simul., 5(3): 861–899. doi: 10.1137/05064182X.

CASTAGNA JP & SUN S. 2006. Comparison of spectral decomposition methods. First Break EAGE, 24: 75–79.

CASTAGNA JP, SUN S & SIEGFRIED RW. 2003. Instantaneous spectral analysis. Detection of low-frequency shadows associated with hydrocarbons. The Leading Edge, 22: 120–132. doi: 10.1190/1.1559038.

CHOI H & WILLIAMS WJ. 1989. Improved time-frequency representation of multicomponent signals using exponential kernels. IEEE Transactions on Acoustics, Speech, and Signal Processing, 37: 862–871. doi: 10.1109/ASSP.1989.28057.

COHEN L. 1989. Time-frequency distributions – a review. Proceedings of the IEEE, 77: 941–981. doi: 10.1109/5.30749.

FRANCO AWP, MORAES FS & THEODORO CE. 2015. Multicomponent seismic data conditioning and joint PP-PS inversion. In: 14th International Congress of the Brazilian Geophysical Society & EXPOGEF, Rio de Janeiro, Brazil, 390–394. doi: 10.1190/sbgf2015-076.

KJARTANSSON E. 1979. Constant Q-Wave Propagation and Attenuation. Journal of Geophysical Research: Solid Earth, 84: 4737–4748. doi: 10.1029/JB084iB09p04737.

LI Y, ZHENG X & ZHANG Y. 2011. High-frequency anomalies in carbonate reservoir characterization using spectral decomposition. Geophysics, 76: V47–V57. doi: 10.1190/1.3554383.

LIU Y & FOMEL S. 2013. Seismic data analysis using local time-frequency decomposition. Geophysical Prospecting, 61: 516–525. doi: 10.1111/j.1365-2478.2012.01062.

LUPINACCI WM & OLIVEIRA SAM. 2015. Q factor estimation from the amplitude spectrum of the time-frequency transform of stacked reflection seismic data. Journal of Applied Geophysics, 114: 202–209. doi: 10.1016/j.jappgeo.2015.01.019.

MALLAT SG & ZHANG Z. 1993. Matching pursuits with time-frequency dictionaries. IEEE Transactions on Signal Processing, 41: 3391–3415. doi: 10.1109/78.258082.

PARTYKA G, GRIDLEY J & LOPEX J. 1999. Interpretational applications of spectral decomposition in reservoir characterization. The Leading Edge, 18: 353–360. doi: 10.1190/1.1438295.

ROJAS NA. 2008. Spectral decomposition applied to time-lapse seismic interpretation at Rulison field, Garfield County, Colorado. Colorado School of Mines Dissertation.

SINHA S, ROUTH PS & ANNO PD. 2005. Spectral decomposition of seismic data with continuous-wavelet transform. Geophysics, 70: 19–25. doi: 10.1190/1.2127113.

WU X & LIU T. 2009. Spectral decomposition of seismic data with reassigned smoothed pseudo Wigner-Ville distribution. Journal of Applied Geophysics, 68: 386–393. doi:10.1016/j.jappgeo.2009.03.004.

Recebido em 24 abril, 2017 / Aceito em 30 maio, 2017
Received on April 24, 2017 / Accepted on May 30, 2017